Journal of Optoelectronics and Advanced Materials Vol. 4, No. 3, September 2002, p. 799 - 808

LEAD-CADMIUM OXYFLUORIDE GLASSES AND GLASS-CERAMICS

M. A. P. Silva[a]*, V. Briois[b], M. Poulain[c], Y. Messaddeq[d], S. J. L. Ribeiro[d]

[a] POMA UMR CNRS 6136, Université d'Angers, 2 bd. Lavoisier, 49045 Angers, France
* Corresponding author. E-mail: mauricio.silva@univ-angers.fr
[b] LURE, Bât. 209-d, Université Paris-Sud, BP 34, 91898, Orsay Cedex France.
[c] CEMA, Université de Rennes I, 35042 Rennes, France.
[d] Instituto de Química- UNESP, CP. 355, CEP 14801-970, Araraquara, SP, Brazil.

Glasses and glass-ceramics have been obtained in oxyfluoride systems involving lead and cadmium fluorides and one of the well-known glass former oxides SiO_2, B_2O_3 and TeO_2. Vitreous domains were established and a wide range of compositions including high heavy metal contents lead to stable glasses. Amorphous structures have been studied by short-range order spectroscopy techniques (Raman scattering and x-ray absorption) and molecular basic structures have been identified. Besides the usual oxides, the role of glass former could also be proposed for cadmium ions. Special attention has been paid for crystallization process. Cubic lead fluoride, cubic lead tellurite, tetragonal tellurium oxide and a solid solution of the type $Pb_{1-x}Cd_xF_2$ are obtained as crystallization products depending on the composition and temperature of heat treatments. $Pb_{1-x}Cd_xF_2$ solid solutions are well known superionic materials and obtaining this solid solution as a crystal phase could be very interesting for applications concerning ionic electrical conduction properties. The addition of rare earth ions led to the control of the crystallization process. In the presence of the nucleating ion only the cubic form β-PbF_2 was identified. Rare earth ions are present in the crystal phase and crystal-like spectroscopic properties were observed suggesting interesting applications for these perfectly transparent glass ceramics in photonics.

(Received July 11, 2002; accepted July 22, 2002)

Keywords: Oxyfluoride glasses, Glass-ceramics, Structure

1. Introduction

Oxyfluoride glasses are well known for many years, but our interest in this kind of material has grown after the demonstration in the literature [1] of the possibility of obtaining the so-called rare earth containing ultratransparent glass-ceramics. Besides the importance of oxyfluoride glasses and glass ceramics as technological materials, e.g. in photonics, a lack in systematic glass formation study, with the determination of vitreous domains, and structural studies, including spectroscopic techniques is observed. Moreover, there is the possibility to get hybrid materials displaying fluoride and/or oxide properties depending on the compositions, but the synergetic effects of these somewhat two phase materials are still a challenge to be explored in materials science.

This paper attempts to review our last woks in the synthesis, rare earth doping and structural and optical characterization of lead-cadmium oxyfluoride glasses and glass-ceramics [2-4]. Results from Differential Scanning Calorimetry (DSC), X-Ray Diffraction (XRD), Er^{3+} Luminescence and Extended X-ray Absorption Fine Structure (EXAFS) are reproduced here for glasses and glass-ceramics in the systems PbF_2-CdF_2-SiO_2, PbF_2-CdF_2-B_2O_3 and PbF_2-CdF_2-TeO_2.

Glasses have been obtained by the conventional melting and casting glass techniques, in room atmosphere. In addition to the relatively simple preparation method and optical characteristics of rare earth (RE) doped samples, very interesting devitrification (glass crystallization) features are presented

by these systems. For example, the PbF_2-CdF_2-SiO_2 and PbF_2-CdF_2-B_2O_3 glasses are characterised by the devitrification of the cubic form of lead fluoride, β-PbF_2, with the possibility of obtaining transparent glass-ceramics under controlled thermal treatments. Rare earth ions may concentrate in the crystalline phase and so their spectroscopic properties appear mainly with crystal-like features. $Cd_{1-x}Pb_xF_2$-type solid solutions where also identified in some devitrified samples. On the other hand, PbF_2-CdF_2-TeO_2 glass-crystallization leads to the formation of a transparent glass-ceramic, in which the first crystalline phase, the cubic lead tellurite $PbTe_3O_7$ decomposes into α-TeO_2 at higher temperature.

2. Experimental

Glasses were prepared by conventional melting and casting techniques. Starting materials were ground together and melted in open platinum crucibles in electric furnaces at temperatures ranging from 800-1100ºC depending on the composition. Melts were quenched to room temperature between brass pieces. Glass formation was identified by considering together the visual inspection for crystalline-like phases, the amorphous character to the x-rays and the identification of glass transition temperature (Tg) followed by the crystallization of the supercooled liquid (Tx and Tp) in DSC curves.

Differential scanning calorimetry (DSC) curves were obtained from powdered samples in aluminum pans under N2 atmosphere in a TA equipment. Heating rate of 10ºC/min was routinely used. X-ray diffractograms were obtained from powdered samples with a Siemens diffractometer with the Cu K_α line. A step mode (2θ) with integration time of 2s was used. X-ray absorption spectra were obtained at D44 beam line of LURE (France). EXAFS spectra were obtained at the Pb L_{III}-edge (13035 eV), Cd K-edge (26711 eV) and Te K-edge (31814 eV) in the transmission mode at liquid nitrogen temperature (77K). Details in the experimental set-ups during absorption spectra acquisition (monochromators, ionization chambers, time steps for acquisition) were described in previous papers [2-4].

X-ray absorption data have been analyzed by conventional methods including normalization, background removal and Fourier Transform. Data analysis was performed using the "EXAFS pour le Mac" simulation program [5]. To determine the structural parameters *R*, *N* and σ (absorbing atom's first neighbors distance, coordination numbers and Debye-Waller factors respectively) the filtered Fourier transformed EXAFS signal was treated as a sum of sinusoidal wave functions using the standard EXAFS equation:

$$k\chi(k) = S_0^2 \sum_i \frac{N_i}{R_i^2} e^{-2k^2\sigma_i^2} e^{-\frac{2R_i\Gamma}{k}} f_{ij}(\pi,k)\sin\left[2kR_i + \Phi_{ij}(k)\right], \quad (1)$$

where $\lambda(k)$ is the photoelectron mean free path ($\lambda = k/\Gamma$), and $f_i(\pi,k)$ and $\Phi_i(k)$, the amplitude and the phase functions for this coordination shell, which have been tabulated by McKale [6] or obtained experimentally from standard compounds. In this case, starting reagents CdF_2 (cubic), β–PbF_2 (cubic), β–PbO (orthorhombic) and α–TeO_2 (tetragonal) were used during spectra analysis as reference compounds.

3. Results and discussions

With the criteria of glass formation listed above, vitreous domains with homogenous and clear samples could be identified for the investigated systems. Fig. 1 shows the resulting composition diagrams and Table 1 shows some values of characteristic temperatures obtained by DSC. Fig. 2 shows the X-ray diffraction spectra obtained for the glassy and glass ceramics samples of all systems. In the following sessions we show the main results obtained from each system separately. For a more detailed description of methods, results and discussions, we would like to send the reader to the main cited references.

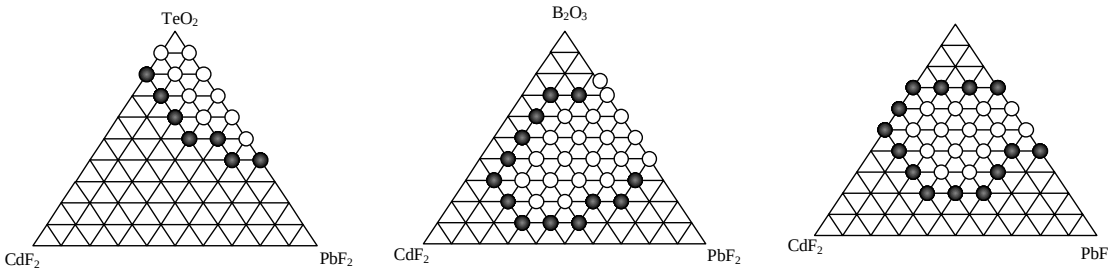

Fig. 1. Vitreous domain diagram for the systems studied. Experimental condition indicated in the text. Binary B_2O_3-PbF_2 glasses: Gressler, C. A. and Shelby, J. E.; J. Appl. Phys . 66 (3) 1989.

Table 1. Characteristics temperatures (ºC) and (T_x-T_g) parameter obtained by thermal (DSC/DTA) for some glasses of the studied systems. T_g: glass transition temperature; T_x: temperature of beginning of the crystallization; T_p: temperature of maximum crystallization rate (peak temperature). Heating rate q = 10 ºC.min^{-1}.

Composition	T_g	T_x	T_p	(T_x-T_g)
$50SiO_2$-$50PbF_2$	273	333	369	61
$50SiO_2$-$30PbF_2$-$20CdF_2$	343	467	510	124
$50SiO_2$-$10PbF_2$-$40CdF_2$	419	504	541	85
$45B_2O_3$-$35PbF_2$-$20CdF_2$	356	516	530	160
$40B_2O_3$-$30PbF_2$-$30CdF_2$	360	509	538	149
$35B_2O_3$-$25PbF_2$-$40CdF_2$	372	495	514	117
$50TeO_2$-$50PbF_2$	189	196	208	7
$70TeO_2$-$30PbF_2$	236	251	258	15
$90TeO_2$-$10PbF_2$	272	294	299	22
$90TeO_2$-$10CdF_2$	309	327	329	18
$80TeO_2$-$10PbF_2$-$10CdF_2$	273	296	299	23

3.1. PbF_2-CdF_2-SiO_2

A relatively large glass forming area is observed in the PbF_2-CdF_2-SiO_2 ternary system. The incorporation of cadmium and lead fluoride in silica glass network results in a large decrease of the glass transition temperature. This involves two different mechanisms: first, fluorine anions which are considered as non-bridging reduce the network connectivity; second, heavy cations act classically as modifiers, which also decreases T_g. The influence of the Cd^{2+} to Pb^{2+} ratio on T_g value is noteworthy, as T_g values raise significantly when Cd^{2+} substitutes Pb^{2+} (Table 1). We assume that Cd^{2+} ions enter the vitreous network while Pb^{2+} ions act mainly as modifiers.

All glasses obtained are amorphous under X-rays. Partially crystallized samples were obtained by submitting the glass of molar composition $30PbF_2$-$30CdF_2$-$40SiO_2$ (“S” sample) and (PbF_2-CdF_2-SiO_2)$_{0.99}$(ErF_3)$_{0.01}$ (“SEr” sample) to 30 (ST1 and SErT1) and 60 (ST2 and SErT2) minutes heat treatments at the T_x temperatures obtained from DSC scans. Fig. 2 shows the X-ray diffraction spectra obtained for the samples.

Samples S and ST1 are amorphous. The ST2 sample, on the contrary, presents relatively intense peaks that could be easily assigned to the β-PbF_2 cubic phase (a = 5.94 Å). Some less intense peaks, marked with an asterisk in the Fig. 2, could be assigned to a solid solution of the type (Cd_xPb_{1-x})F_2. The cubic cell parameter obtained from the peak positions is 5.70 ± 0.02 Å.

For the sample SEr small diffraction peaks can be discerned from the base glass which positions agree with the β-PbF_2 pattern. With heat treatments (SErT1 and SErT2) only this phase can be identified. Peak positions however are shifted and a cubic cell parameter of 5.88 ± 0.02 Å is obtained. These crystallization features, when erbium ions are present, indicate the important role of

nucleating agent for the β-PbF_2 played by erbium, but also that the RE ions are present in the crystalline phase, reflected by the shift in the cubic cell parameter.

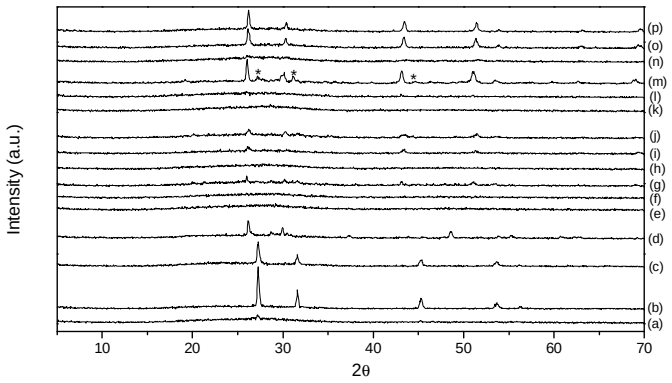

Fig. 2. X-ray diffractograms of samples: (a) T; (b) TT1; (c) TT2; (d) TT3; (e) B; (f) BT1; (g) BT2; (h) BEr; (i) BErT1; (j) BErT2; (k) S; (l) ST1; (m) ST2; (n) SEr; (o) SErT1 and (p) SErT2;. Stars indicate the $Cd_xPb_{(1-x)}F_2$ solid solution related peaks in sample ST2.

Fig. 3 presents the |F(r)| curves obtained from EXAFS spectra at the Pb L_{III} absorption edge for the samples studied. For samples S, ST1 and SEr only a first shell peak is observed at 1.6 Å with a clear shoulder at 2.0 Å. For samples ST2, SErT1 and SErT2 the main first peak appears shifted towards larger distances (at 2.1 Å) and a small peak is observed at 1.5 Å. Furthermore,1 a second broad and intense peak appears in the 4.0 to 4.9 Å range. All structural results obtained for the Pb^{2+} L_{III}-edge are gathered in Table 2.

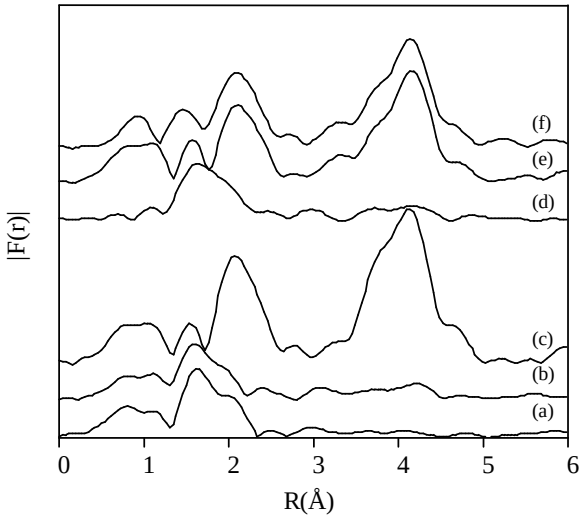

Fig. 3. |F(r)| curves obtained at the Pb L_{III} -edge for the samples: (a) S; (b) ST1; (c) ST2; (d) SEr; (e) SErT1 and (f) SErT2.

A multi-shell fitting procedure was adopted for samples S, ST1 and SEr, with phase and amplitude functions obtained from McKale tables [6]. In the undoped glass, Pb^{2+} ions are surrounded by a first shell with 4 to 5 first neighbor atoms located in 2 sub-shells at relatively short distances (2.3-2.4 Å). When Er^{3+} ions are added ("SEr" glass), 2.3 atoms (at 2.3 Å) are obtained for the first sub-shell

while 4.3 atoms (at 2.5 Å) are observed for the second sub-shell. This distance is also longer than the one observed for the "S" glass suggesting a more important contribution from F^- ions in the EXAFS signal.

Table 2. EXAFS results at the Pb L_{III} edge on glasses and glass ceramics in the system PbF_2-CdF_2-SiO_2.

	First shell						Second shell	
	S	**ST1**	**ST2**	**SEr**	**SErT 1**	**SErT 2**	**ST2**	**SErT2**
N	2.1	2.3	5.4	2.3	4.7	5.5	1.0(Cd)	-
	2.5	2.7		4.3			4.4(Pb)	3.3(Pb)
							24.0(F)	19.4(F)
σ(Å)	0.120	0.123	0.148	0.123	0.156	0.165	0.077	-
	0.154	0.166		0.172			0.088	0.084
							0.146	0.159
R(Å)	2.29	2.28	2.58	2.31	2.57	2.57	4.03	-
	2.39	2.44		2.46			4.20	4.19
							4.91	4.88
ΔE_0(eV)	3.6	2.6	-0.4	3.2	0.0	-0.6	2.0	-
	8.4	7.7		7.6			-3.0	-2.2
							-0.3	-0.7
ρ(×10^{-3})	5.5	4.0	5.1	4.7	3.8	2.2	5.3	1.2

The main first peak of |F(r)| for the crystallized samples (ST2, SErT1 and SErT2), was simulated using phase and amplitude functions taken experimentally from β-PbF_2 (N = 8 and R = 2.57 Å). The numerical results indicate the crystallization of this cubic fluoride. Nevertheless, the small peak at the left side of the first peak for ST2, SErT1 and SErT2 indicates the presence of a second family of Pb^{2+} ions included in the glass network, probably surrounded by oxygen atoms. In fact that is the role suggested for Pb^{2+} ions in the non-crystallized samples S, ST1 and SEr.

The second main peak observed in the F(r) curves of the crystallized samples is related, in the β-PbF_2 structure, to the 12 Pb^{2+} atoms at 4.19Å and 24 F^- atoms at 4.91Å, at the second lead coordination shell. Table 2 shows a satisfactory result for sample SErT2. As evidenced before from XRD results, a $(Cd_xPb_{1-x})F_2$ solid solution was observed in the sample ST2, and no such a good fit could be obtained for this sample, considering only the Pb and F atoms in the second shell. Cadmium atoms were then included in the fitting procedure and an excellent fit was obtained. Cd^{2+} ions are located at about 4.03Å from the central Pb^{2+} atom in the average cubic cell. In such a $(Cd_xPb_{1-x})F_2$ solid solution, the shortening of Pb-Cd distances (4.03Å) compared to Pb-Pb distances (4.19Å) is totally expected due to the smaller Cd^{2+} ionic radius (R_{Cd}= 109 pm) compared to that of Pb^{2+} ions (R_{Pb}= 133 pm).

Fig. 4 shows the Fourier transform |F(r)| curves of the EXAFS signal obtained for the samples at Cd K-edge. These |F(r)| curves, which express the short range ordering, do not show any structure indicating a medium or long range ordering. Quantitative simulation shows that either for the glasses or the glass-ceramics, the first Cd^{2+} ions coordination shell is composed of 4 atoms at about 2.26±0.02Å, distance significantly shorter than those found in cubic CdF_2 (8F at 2.33Å). One assumes that the change in Cd^{2+} environment between the crystalline starting materials and the glass should occur *via* a double decomposition in the melt, according to the general reaction:

$$SiO_2+2CdF_2 \rightarrow SiF_4+2CdO \quad (2)$$

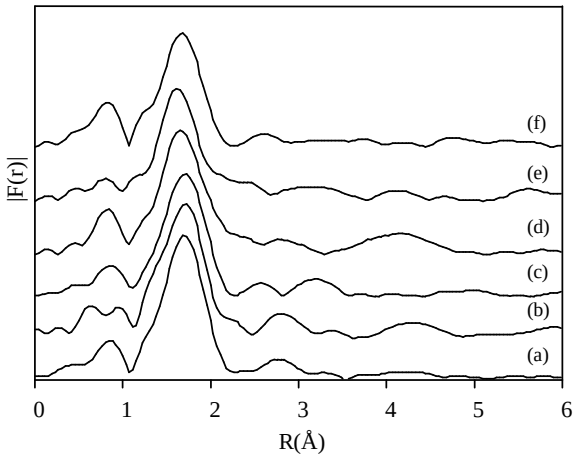

Fig. 4. |F(r)| curves obtained at the Cd K-edge for the samples: (a) S; (b) ST1; (c) ST2; (d) SEr; (e) SErT1 and (f) SErT2.

These new [CdO_4] units formed in this way could enter the vitreous network structure constructed from the SiO_4 tetrahedra. This arrangement is likely to remain in the crystallized samples. Fig. 5 shows Er^{3+} emission spectra obtained under excitation at 378nm (Er^{3+} $^4I_{15/2}\rightarrow{}^4G_{11/2}$ absorption transition). The $^4I_{13/2}\rightarrow{}^4I_{15/2}$ transition is observed with the typical inhomogeneously broadened spectrum, due to the statistical distribution of sites, for the base glass (Fig. 5(a)). After heat treatment well resolved lines are clearly observed (Fig. 5(b)). Fig. s 5(c-d) show spectra obtained before in our laboratory for a lead-cadmium fluorogermanate transparent glass-ceramic [7] and the lead–cadmium fluoroborate glass-ceramic for comparison purposes. These results are in total agreement with the ones obtained by XRD and EXAFS, as the spectra from Fig. 5(b-d) could be assigned to Er^{3+} doped β-PbF_2 crystals [7].

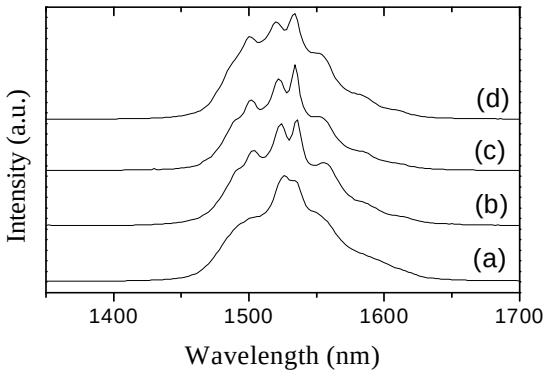

Fig. 5. Room temperature Er^{3+} $^4I_{13/2}\rightarrow{}^4I_{15/2}$ emission spectra obtained under 370 nm excitation. (a) SEr; (b) SErT2; (c) Transparent glass ceramic in the system $PbGeO_3$-PbF_2-CdF_2 [7]; (d) Glass ceramic in the system B_2O_3-PbF_2-CdF_2 (BErT2).

3.2. PbF_2-CdF_2-B_2O_3

Very stable glasses could also be obtained in this system. As Table 1 shows, values around 160ºC for the (T_x-T_g) parameter could be obtained. Structure and crystallization processes have been studied by X-ray diffraction and EXAFS analysis at the Pb L_{III} and Cd K edges [3]. The structural

roles of these atoms are close to those of the system with SiO_2. But, under similar thermal conditions, the crystallization of β-PbF_2 in this system is less complete than the one on fluorosilicate system, as concluded from the weak intensity of the XRD peaks (Fig. 2), and the amorphous character of the EXAFS spectra obtained at Pb L_{III} edge. Moreover, differently from the fluorosilicate system, there is no evidence of formation of $(Cd_xPb_{1-x})F_2$ solid solutions during heating of the glass, and the optical properties of the erbium doped glass ceramics are those observed for a Er^{3+} doped β-PbF_2 crystals (Fig. 5).

3.3. PbF_2-CdF_2-TeO_2

Homogeneous, thin glassy samples, typically 1.0 mm in thickness, were obtained in the TeO_2 rich portion of the diagram**.** Fig. 6 shows a DSC thermogram for the glass of molar composition $10PbF_2$-$10CdF_2$-$80TeO_2$, labeled "T" sample [4]. The evolution of the glass transition temperature (Table 1) versus composition exemplifies the structural role of the modifiers compounds. The comparison of the Tg values for the TeO_2-PbF_2 glasses from this study and the TeO_2-PbO glasses reported previously [8] shows that the Tg drop is larger when PbF_2 is used, i.e. the "modifier" role played by PbF_2 is more pronounced that the one observed for PbO. This may be explained as it leads to a larger number of non-bridging anions. It is also more important than the effect induced by CdF_2 as it may be seen comparing $90TeO_2$-$10PbF_2$ and $90TeO_2$-$10CdF_2$ glasses.

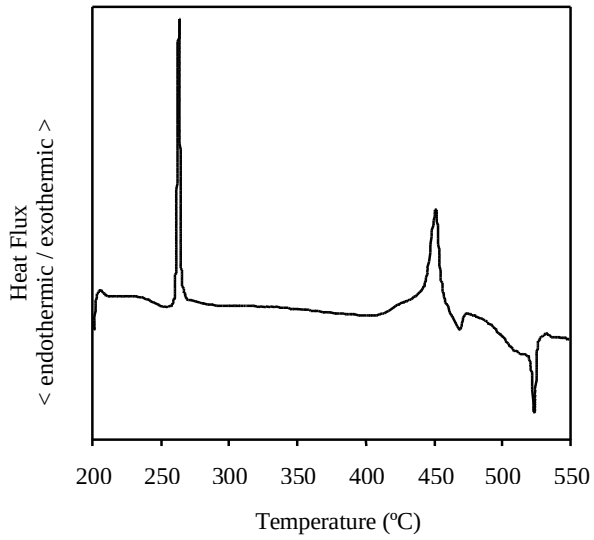

Fig. 6. Differential scanning calorimetry thermogram of the "T" sample, of composition (in mol%) $80TeO_2$-$10CdF_2$-$10PbF_2$. Heating rate $q=10ºC.min^{-1}$.

For the glass-ceramics preparation, heat treatments were performed as follow: sample "T" was submitted to a heat treatment at 300ºC for 30 minutes, which is just above the first crystallization peak observed in the DSC curve (Fig. 6). This heat treated sample will be called hereafter "TT1". The sample "T" was also heat treated for 5 and 60 minutes at 400ºC which is just before the second crystallization peak observed in Fig. 6. These two heat treated samples are called hereafter "TT2" and "TT3". Sample TT1 appears as a yellowish transparent block, with no visible crystallization. Sample TT2 displays crystallization at the surface and sample TT3 shows a completely white opaque body.

Fig. 7(a-d) shows the Raman spectra obtained for glassy samples $90TeO_2$-$10PbF_2$, $70TeO_2$-$30PbF_2$, $50TeO_2$-$50PbF_2$ and also $80TeO_2$-$10PbF_2$-$10CdF_2$. Fig. 7(e and f) shows the Raman spectrum obtained for the TT1 and TT3 samples, respectively. For the sake of comparison Fig. 7(g) shows the Raman spectrum obtained for the α-TeO_2. One can easily note the strong similarities between the spectrum obtained for sample TT3 and the one for the α-TeO_2. The bands centered at 450, 650 and 750 cm^{-1} observed in Fig. 7 for the binary TeO_2-PbF_2 glasses have been assigned, respectively, to

the symmetric and antisymmetric vibrations of Te-O-Te linkages and to the stretching vibration between tellurium and non-bridging oxygen atoms like in TeO_3 tp or TeO_{3+1} polyhedra [12]. Fig. 7 shows that, as PbF_2 content increases, the intensity of the bands located at 450 and 650 cm^{-1} decreases, at the expenses of the relative increase in intensity of the band at 750 cm^{-1}. These results describe the changes in the tellurium coordination polyhedra from TeO_4 tbp to TeO_3 tp with increasing lead/cadmium fluorides.

X-ray diffraction patterns obtained for these samples are shown in Fig. 2. As stated before, sample TT1 is completely transparent. However well defined diffraction peaks could be observed in DRX curves. The diffraction patterns were compared with data from JCPDF (Joint Commission on Powder Diffraction Files) and a good agreement was found between the diffractogram obtained for the transparent sample TT1 and the cubic (a = 5.650Å) $PbTe_3O_7$ (File # 37-1392). This phase is described in the literature as an "antiglass" phase where order exists only at long distance and an important dispersion in the tellurium first neighbors distances is observed [9]. This "antiglass" character is in fact confirmed by the Raman spectrum presented in Fig. 7(e). The high frequency bands involving Te-O modes in the 550-850cm^{-1} range, are inhomogenously broadened in the same way observed for the mother glass (Fig. 7(b)). Tetragonal form of tellurium oxide, α-TeO_2 (File#42-1365), was identified as the main crystalline phase in sample TT3. The increase in the temperature leads to the dissolution or decomposition of the cubic $PbTe_3O_7$ phase in the matrix, giving rise to tetragonal α-TeO_2.

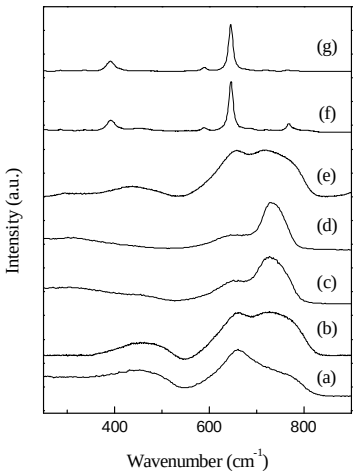

Fig. 7. Raman spectra for the samples: (a) $90TeO_2$-$10PbF_2$; (b) sample "T" ($80TeO_2$-$10CdF_2$-$10PbF_2$); (c) $70TeO_2$-$30PbF_2$; (d) $50TeO_2$-$50PbF_2$; (e) sample "TT1" (300 ^oC / 30 minutes); (f) sample "TT3" (400^oC/60 minutes); (g) α - TeO_2.

Fig. 8 shows the modulus of the Fourier Transform, |F(r)|, curves, not corrected for phase shift, obtained from EXAFS signals at the Te K-edge in samples T, TT1 and TT3, and reference α-TeO_2. The first peak, at about 1.46 Å, is relative to the first coordination shell around tellurium atoms, which is composed, in α-TeO_2, by the oxygen atoms in TeO_4 tbp units, i.e. two at 1.90 Å (equatorial position) and two at 2.08 Å (axial positions) [10]. The second peak, at about 3.57 Å corresponds to the second Te coordination shell, composed by four tellurium atoms at 3.74 Å, two at 3.83 Å and four at 4.07 Å. Simulations of the EXAFS signal relative to each shell were made using a multi-subshell fitting procedure. The first coordination sphere was better simulated considering two slightly different Te-first neighbors distances. For the second Tellurium coordination sphere a 3 sub-shells simulation was necessary. Table 3 gives the numerical results obtained from simulations, which describe the Te first shell environment as been close to the one found in reference paratellurite, in all samples. The same is observed for the second Te coordination shell in TT3 sample. This result is supported by X-ray diffraction observations. However, while vibrational spectroscopy shows a mixture of TeO_4 tbp and TeO_3 tp unities, mainly in samples T and TT1, X-ray absorption indicates that TeO_4 tbp appears as a majority proportion. In fact, a mixture of entities must be considered since relative Raman Scattering cross-sections are not known for the two structures (if the force constant in the tp structure is very important, then a little fraction of tp unites can strongly interfere the Raman signal).

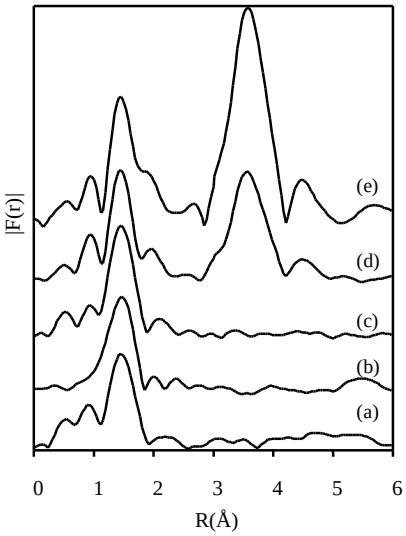

Fig. 8. |F(r)| curves obtained at the Te K-edge for the samples: (a) T; (b) TT1; (c) TT2; (d) TT3 and (e) α-TeO_2.

Table 3. EXAFS results at the Te K edge on glasses and glass ceramics in the system PbF_2-CdF_2-TeO_2.

	First shell				Second shell
	T	**TT1**	**TT2**	**TT3**	**TT3**
N	2.1	1.82	1.9	1.8	3.9
	2.0	1.8	2.0	2.1	2.6
					4.0
σ (Å)	0.06	0.05	0.04	0.03	0.076
	1	2	7	6	0.129
	0.08	0.08	0.08	0.07	0.099
	6	6	0	3	
R (Å)	1.92	1.91	1.91	1.90	3.74
	2.08	2.08	2.07	2.08	3.87
			2		4.03
ΔE_0(eV)	4.6	2.3	5.0	4.3	-1.3
	4.3	5.6	7.4	2.5	-3.4
					0.7
$\rho(\times 10^{-3})$	6.9	4.8	7.7	10	19

Cadmium K-edge EXAFS studies were performed in T, TT1 and TT3 samples. As in the precedent cases, with the fluorosilicate and fluoroborate systems, cadmium environment changes drastically by comparison to the cubic CdF_2 reference. Cd K-edge results indicate a diminution on the coordination number from 8 in the cubic CdF_2 cell to 4 in the samples. The asymmetry of peaks in the |F(r)| curves reveals also the anionic distance distribution around cadmium atoms. Anion distributions are centered on mean distances varying between 2.27 and 2.29Å (samples T and TT1, respectively) and 2.35Å (sample TT3) [4]. As in the case of fluorosilicates and fluoroborates, these differences in the first coordination shell of samples and start compound CdF_2 could be well explained by the formation of $[CdO_4]$ units, following the reaction:

$$TeO_2+2CdF_2 \rightarrow TeF_4+2CdO \quad (3)$$

Lead L_{III}-edge EXAFS studies were also performed in T, TT1, TT2 and TT3. Asymmetric peaks were obtained in the |F(r)| curves, reflecting the occurrence of a large atomic distance distribution in lead surroundings. Multi-shell fitting procedure was adopted and a two sub-shell environment for lead cations was found, in which anions are located around two main average distances, at about 2.3 and 2.5 Å. For the

transparent glass-ceramic (sample TT1) we have assigned [4] a structure appearing around 3.49 Å (uncorrected for phase shift) to Te-Pb contribution from the $PbTe_3O_7$ phase. The structure of this kind of compound is characterized by Pb-Te interatomic distance of 3.7 Å and Pb-Pb distance of 3.9 Å [11].

4. Conclusions

New stable glasses have been synthesized in the PbF_2-CdF_2-MO systems. Lead-cadmium fluorosilicate glass ceramics have been obtained by annealing at 440°C, with β-PbF_2 and a solid solution with the formula $Cd_{0.42}Pb_{0.58}F_2$ as the main crystalline phases. For the three systems presented here, Cd K-edge EXAFS results showed lower coordination numbers and shorter first neighbor distances comparing with the CdF_2 precursor used. This result and the increase of the glass transition temperature observed when Cd^{2+} substitutes for Pb^{2+} suggest the role of glass former played by Cd^{2+} ions and suggests that cadmium ions are preferentially surrounded by oxygen atoms although they were in a fluoride anion environment in the starting material. For fluorosilicate and fluoroborate samples, Pb L_{III}-edge EXAFS analysis suggests at least two families of sites for Pb^{2+} ions. The first one observed for the mother glass with Pb^{2+} coordination numbers and first neighbor distances close to the values found for β-PbO. In crystallized samples this first family of sites is still present, but a fluoride containing first coordination shell is also observed. Crystallization experiments showed the inclusion of Er^{3+} ions in the β-PbF_2 crystalline phase. From EXAFS and XRD results we could estimate the crystalline content to be from 30 to 40% of the initial Pb^{2+} content in the fluorosilicate system [2]. No Pb-Cd solid solution could be observed in that case, suggesting the role of nucleation agent for the PbF_2 phase played by Er^{3+} ions. Near infrared emission spectra showed crystal-like spectra with the narrowing of the emission lines by comparing with the one observed for mother glass. Concerning the fluorotellurite system, Raman scattering results show the increase of the number of structural units described as [TeO_3] trigonal pyramids and [TeO_{3+1}] polyhedra at the expense of the [TeO_4] trigonal bipyramids supposed to exist in the TeO_2 rich samples. Heat treatments performed at 300°C for the $10PbF_2$-$10CdF_2$-$80TeO_2$ (mol%) sample reveal the possibility of obtaining transparent glass-ceramics in which the $PbTe_3O_7$ crystalline phase could be identified by x-ray diffraction and EXAFS measurements performed at the Te K, Cd K and Pb L_{III} edges. Annealing at larger temperatures leads to the decomposition of this crystalline phase and the final material consists in a mixture of phases among which one of them could be identified as the α-TeO_2.

References

[1] P. Tick, M. Dejneka. in Proceedings of the International Congress on Glass, 18, 1998, July 5-10, p.1.
[2] M. A. P. Silva, S. J. L. Ribeiro, Y. Messaddeq, V. Briois, M. Poulain, in Press, available online 18 June 2002, Journal of Physics and Chemistry of Solids.
[3] M. A. P. Silva, S. J. L. Ribeiro, Y. Messaddeq, V. Briois, M. Poulain, J. Brazil. Chem. Soc. **13**(2), 200 (2002).
[4] M. A. P. Silva, Y. Messaddeq, V. Briois, M. Poulain, F. Villain, S. J. L. Ribeiro, Journal of Physics and Chemistry of Solids, **63**(4), 605 (2002).
[5] A. Michalowicz, EXAFS pour le Mac (Societé Française de Chimie, Paris, 1991) p. 102.
[6] A. G. McKale, B. W. Veal, A. P. Paulikas, S. K. Chan, G. S. Knapp, J. Am. Chem. Soc. **110**, 3763 (1988).
[7] L. A. Bueno, P. Melnikov, Y. Messaddeq, S. J. L. Ribeiro, J. Non-Cryst. Solids **247**, 87 (1999).
[8] M. A. P. Silva, Y. Messaddeq, S. J. L. Ribeiro, M. Poulain, F. Villain, V. Briois Journal of Physics and Chemistry of Solids, **62**(6), 1055 (2001).
[9] M. Tromel, H-G. Burckhardt, H. Heydarian, F. W. Hutzler, E. Munch, Acta Crystallogr. A, **40**, 216 (1984).
[10] R. W. Wickoff, Crystal Structures, 2ed. R. E. Krieger Publishing Company, Florida, vol. **1**, 241 (1982).
[11] J. P. Laval (Laboratoire de Matériaux Céramiques et Traitements de Surface, URA CNRS no. 320, Limoges, France) Private Communication.
[12] T. Sekiya, N. Mochida, A. Ohtsuka, J. Non-Cryst. Solids **168**, 106 (1994).